Crystallization mechanism of aluminoferrate glass accompanying a precipitation of nanocrystals of dicalcium ferrite ($Ca_2Fe_2O_5$) and mayenite ($12CaO{\cdot}7Al_2O_3$)

Tetsuaki Nishida,*[a] Shiro Kubuki,[a] Morihiro Shibata,[a] Yonezo Maeda[a] and Toyomi Tamaki[b]

[a]*Department of Chemistry, Faculty of Science, Kyushu University, Hakozaki, Higashiku, Fukuoka 812, Japan*

[b]*Department of Physics, Faculty of Science, Ochanomizu University, Otsuka, Bunkyoku, Tokyo 112, Japan*

Heat treatment of $60CaO{\cdot}27Al_2O_3{\cdot}13Fe_2O_3$ glass resulted in a precipitation of antiferromagnetic dicalcium ferrite ($Ca_2Fe_2O_5$) and mayenite ($12CaO{\cdot}7Al_2O_3$). The effective magnetic moment of the sample decreased from 2.0 to 1.7 μ_B owing to the precipitation of antiferromagnetic particles. The Mössbauer spectrum of the heat-treated sample consisted of two sextets (magnetic hyperfine structure) which were superimposed on two quadrupole doublets. The sextets were assigned to Fe^{3+} occupying octahedral (O_h) and tetrahedral (T_d) sites in the nanocrystals of dicalcium ferrite with a mean diameter >10 nm. The quadrupole doublets were assigned to $Fe^{3+}(T_d)$ occupying Al^{3+} sites in mayenite particles and the glassy phase. IR transmittance of the sample showed a gradual decrease along with the heat treatment. A Johnson–Mehl–Avrami (JMA) plot from the IR-transmission method yielded activation energies (E_a) of 4.9 ± 0.4 and 4.3 ± 0.4 eV for $60CaO{\cdot}27Al_2O_3{\cdot}13Fe_2O_3$ and $60CaO{\cdot}35Al_2O_3{\cdot}5Fe_2O_3$ glasses, respectively. These values are equal to E_a obtained from a Kissinger plot by the DTA method, *i.e.*, 4.2 ± 0.3 and 4.6 ± 0.3 eV, and also to the Al—O bond energy (4.4 eV). These results reveal that crystallization of calcium aluminoferrate glass is triggered by cleavage of Al—O bonds at an early stage in order to form mayenite particles containing Fe^{3+}. After a prolonged heat treatment, the relative absorption area of sextets in the Mössbauer spectra increased at the expense of two doublets. This change suggests a migration of $Fe^{3+}(T_d)$ from mayenite particles and the glassy phase into dicalcium ferrite particles. JMA and Kissinger plots for iron-free $60CaO{\cdot}40Al_2O_3$ glass yielded E_a values of 5.6 ± 0.4 and 6.0 ± 0.3 eV, respectively, equal to the sum of the Al—O (4.4 eV) and Ca—O bond energies (1.4 eV), indicating simultaneous cleavage of Al—O and Ca—O bonds.

Inorganic glasses are generally prepared by quenching the melt of a reagent mixture composed of metal and non-metal oxides. Glass consists of a homogeneous phase, in contrast to crystalline compounds which consist of several crystalline particles separated by grain boundaries. Physical properties of oxide glasses are closely related with the composition, structure and physical properties of each component. Precipitation of crystalline particles in a homogeneous glassy phase, *i.e.*, a structural change from glass to a glass-ceramic, brings about an increase in the mechanical strength. The size and fraction of the crystalline particles in glass-ceramics can be regulated by changing the temperature and time of heat treatment.

It is expected that oxide glasses containing Fe_2O_3 have ferromagnetic or antiferromagnetic properties when several crystalline particles of 'ferrite' precipitate in a paramagnetic glassy phase. 'Ferrite' is expressed by AFe_2O_4, $A_2Fe_2O_5$ *etc.*, in which A refers to a divalent metal ion. The magnetic properties of glass-ceramics can be regulated by changing the temperature and time of heat treatment. This can be advantageous for the development of magnetic materials in which magnetic particles of different sizes are randomly dispersed in a homogeneous glassy phase.

It is interesting to study the short-range structure and physical properties of 'new glasses' such as IR-transmitting, electric conducting, and magnetic glasses, because these properties are closely related with the short-range structure. Aluminate glasses are known to show a high optical transparency in the VIS–IR region and may be utilized as IR-transmitting, IR-regulating or optical memory materials, *etc.* Optical transmittance of aluminate glass in the IR region decreases linearly with the degree of crystallization, since incident light is reflected or scattered by the crystalline particles precipitated in the glassy phase. Using a decreasing rate of the IR transmittance (T) and the Johnson–Mehl–Avrami (JMA) equation, the mechanism of crystallization and activation energy (E_a) can be obtained.[1–4] The JMA equation used in the IR-transmission method, is expressed by

$$\ln[-\ln(1-x)] = n\ln t + \ln k \qquad (1)$$

The volume fraction (x) of the crystalline particles can be approximated by the decreasing rate of T obtained at each stage of heat treatment. The value of n (Avrami index), which reflects the mechanism of crystallization, can be obtained from the slope of the straight line of the JMA plot, *i.e.*, a plot of $\ln[-\ln(1-x)]$ *vs.* heat treatment time (t). Arrhenius plots of rate constants (k), which are obtained from the intercept of the JMA plot, give E_a.

A Kissinger plot in the differential thermal analysis (DTA) is generally used for estimation of E_a of crystallization. The Kissinger equation[5] is expressed by

$$\ln(T_c^2/\alpha) = E_a/RT_c + \text{const.} \qquad (2)$$

in which T_c, α and R are the crystallization peak temperature (in K), heating rate of the sample, and the gas constant, respectively.

The short-range structure of inorganic glasses can be estimated from Mössbauer measurements. As for the structural role of Mössbauer ions in glasses, Nishida *et al.*[6–11] proposed three experimental rules which are useful for the short-range structural study of glasses, as described below.

(1) A linear relationship exists between the glass transition temperature (T_g) and the quadrupole splitting (Δ) of Fe^{3+} which occupies the sites of either network former (NWF) or network modifier (NWM). The 'T_g–Δ rule' states that highly distorted structural units (fragments) require a higher thermal energy for cooperative migration or diffusion[12] in a supercooled liquid. A plot of the T_g *vs.* Δ of Fe^{3+} gives a straight line with a slope of 680 °C mm^{-1} s when Fe^{3+} plays the role of NWF at tetrahedral (T_d) sites such as BO_4, AlO_4, GaO_4, VO_4 and SiO_4.[6–10] The slope of the straight line becomes 260 °C mm^{-1} s when Fe^{3+} occupies octahedral (O_h) NWF sites, as recently observed in tungstate glasses.[11] The slope is even lower, 35 °C mm^{-1} s, when Fe^{3+} occupies NWM sites, as do alkali metal and alkaline-earth metal ions.[6–9] The slope of the straight line in a T_g *vs.* Δ plot will be closely related with the chemical bond strength of the structural units. Since tetrahedra generally

have stronger chemical bonds than octahedra, they will undergo a smaller structural change. A small change of Δ, which indicates a small change of the distortion of Fe^{3+}–oxygen polyhedra, leads to a large slope of 680 °C mm^{-1} s.

(2) The Debye temperature (θ_D) which is obtained from low-temperature Mössbauer measurements is useful for determining the site occupation of Mössbauer ions, since θ_D reflects the chemical bond strength, intermolecular forces, degree of molecular packing, *etc.* The value of θ_D is >280 K when Mössbauer ions like Fe^{3+} and Sn^{4+} occupy NWF sites, while it is lower than 270 K when they occupy NWM sites.

(3) γ-Ray or neutron irradiation of oxide glasses causes a reduction of Fe^{3+} to Fe^{2+} when iron occupies NWF sites. By contrast, Fe^{2+} is oxidized to Fe^{3+} when it occupies NWM sites.

The present study was carried out in order to investigate the crystallization mechanism of $60CaO{\cdot}27Al_2O_3{\cdot}13Fe_2O_3$ glass caused by isothermal annealing. X-Ray powder diffraction (XRD) was used in order to determine the crystalline particles precipitated in the glassy phase. Magnetic susceptibility measurements were performed in order to investigate the change of magnetism due to the precipitation of crystalline particles. Mössbauer and FTIR spectra were measured in order to investigate the change of short-range structure such as the coordination number (CN) of Fe^{3+} and Al^{3+} and the symmetry of oxygen polyhedra. An IR-transmission method combined with a JMA plot was used in order to estimate the mechanism of crystallization and E_a, which was also obtained by DTA (Kissinger plot).

Experimental

Calcium aluminoferrate glass with a composition of $60CaO{\cdot}27Al_2O_3{\cdot}13Fe_2O_3$ was prepared by quenching a melt composed of $CaCO_3$, $Al(OH)_3$ and Fe_2O_3 of guaranteed reagent grade. Before melting, the reagent mixture was pulverized thoroughly in an agate mortar and then transferred into a platinum crucible. After fusion at 1550 °C for 2 h in an electric muffle furnace, a homogeneous glass sample was prepared by quenching the melt with ice-cold water (the outside of the crucible was immersed into ice-cold water). The glass sample was dark brown owing to the presence of iron (Fe^{3+}).

Iron-57 Mössbauer spectra were measured at room temperature with a 10 mCi (3.7×10^8 Bq) $^{57}Co(Pd)$ source. A sheet of metallic iron foil (α-Fe) enriched with ^{57}Fe was used as the reference for the isomer shift, δ, and for calibrating the velocity scale of the spectrometer and spectral analysis was by a least-squares method. The FTIR absorption spectra were measured using the conventional KBr disk method, while transmission spectra were obtained using glass samples. Glass transition temperatures (T_g) and crystallization peak temperatures (T_c) were determined by DTA conducted at a heating rate of 5 °C min^{-1}, using powdered α-Al_2O_3 as the standard. In addition, DTA was conducted at different heating rates in order to determine E_a from a Kissinger plot. XRD patterns were recorded at a scanning rate of 2° min^{-1} with Cu-Kα radiation. Magnetic susceptibility measurements were conducted using the Faraday method over the temperature range 80–300 K under an external magnetic field of 8 kG, and $HgCo(NCS)_4$ was used as the calibrant. The effective magnetic moment (μ_{eff}) was calculated from

$$\mu_{eff} = (8\chi_m T)^{1/2} \quad (3)$$

in which χ_m and T are the molar magnetic susceptibility and the temperature (in K), respectively.

Results and Discussion

Homogeneous glass samples could be prepared in the $60CaO{\cdot}(40-x)Al_2O_3{\cdot}xFe_2O_3$ system when the Fe_2O_3 content (x) was ⩽13 mol%. The formation of homogeneous glass samples was confirmed by XRD, as illustrated in Fig. 1(a). The XRD pattern has a halo peak at *ca.* 20–30°, as is generally observed in several oxide glasses with an 'amorphous' structure. Isothermal annealing of the $60CaO{\cdot}27Al_2O_3{\cdot}13Fe_2O_3$ glass at a temperature close to T_c (783 °C) resulted in precipitation of crystalline particles. XRD patterns of samples heat treated at 750 °C for 2000 and 5000 min are shown in Fig. 1(b) and 1(c), respectively. Several diffraction peaks due to dicalcium ferrite ($Ca_2Fe_2O_5$) and mayenite ($12CaO{\cdot}7Al_2O_3$) are observed together with a few diffraction peaks due to brownmillerite ($4CaO{\cdot}Al_2O_3{\cdot}Fe_2O_3$). Structural changes of AlO_4 and FeO_4 tetrahedra were observed by FTIR, as shown in Fig. 2. A broad absorption peak due to Al—O stretching band of AlO_4 tetrahedra was observed at *ca.* 790 cm^{-1} in the original glass [Fig. 2(a)] and shifted gradually towards higher wavenumbers up to 840 cm^{-1}, with increasing crystallization. This shift indicates a decrease in the mean Al—O bond length and an increase in the chemical bond strength or 'force constant'. The peak shift of the Al—O stretching band towards higher wave-

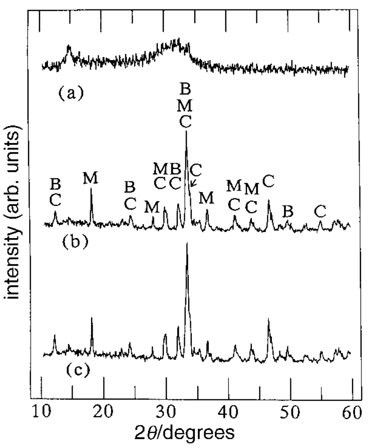

Fig. 1 XRD patterns of $60CaO{\cdot}27Al_2O_3{\cdot}13Fe_2O_3$ after heat treatment at 750 °C for (a) 0, (b) 2000 and (c) 5000 min. The diffraction peaks labelled C, M and B refer to dicalcium ferrite, mayenite, and brownmillerite, respectively.

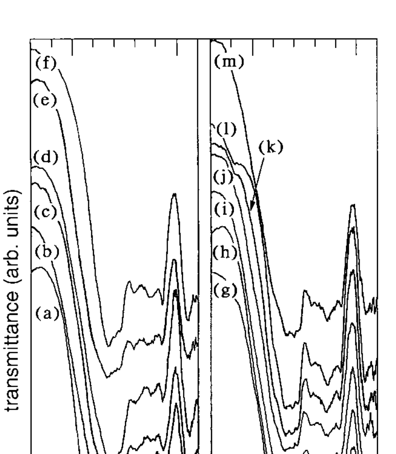

Fig. 2 FTIR absorption spectra of $60CaO{\cdot}27Al_2O_3{\cdot}13Fe_2O_3$ after heat treatment at 750 °C for (a) 0, (b) 50, (c) 100, (d) 200, (e) 300, (f) 500, (g) 700, (h) 1000, (i) 1500, (j) 2000, (k) 3000, (l) 4000 and (m) 5000 min

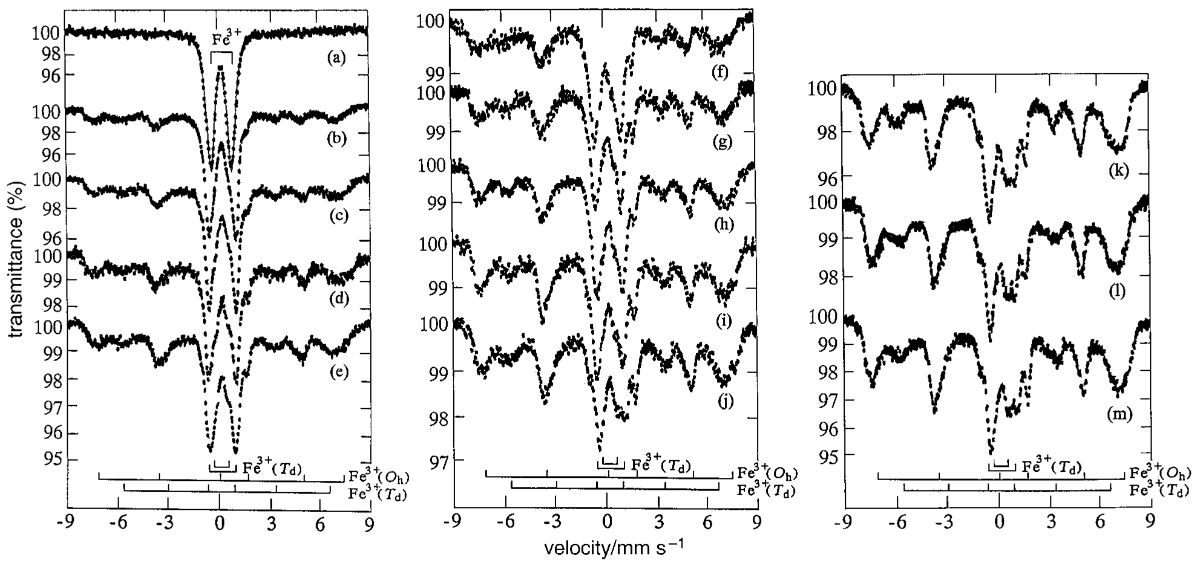

Fig. 3 ^{57}Fe Mössbauer spectra of $60CaO{\cdot}27Al_2O_3{\cdot}13Fe_2O_3$ after heat treatment at 750 °C for (a) 0, (b) 50, (c) 100, (d) 200, (e) 300, (f) 500, (g) 700, (h) 1000, (i) 1500, (j) 2000, (k) 3000, (l) 4000 and (m) 5000 min

number is ascribed to the formation of mayenite particles, as observed in a $60CaO{\cdot}35Al_2O_3{\cdot}5Fe_2O_3$ glass.[13] FTIR spectra of heat-treated samples [Fig. 2(b)–2(m)] showed a new peak at 580 cm^{-1} ascribed to $Fe^{3+}(T_d)$ in $Ca_2Fe_2O_5$. It is known that $Ca_2Fe_2O_5$ crystals contain equal numbers of $Fe^{3+}(O_h)$ and $Fe^{3+}(T_d)$.[14–20] Fig. 2 reveals that a local structural change of aluminoferrate glass could be detected after heat treatment for 50 min.

Precipitation of crystalline particles in the glassy phase was investigated by Mössbauer spectroscopy. While the Mössbauer spectrum of the original glass sample [Fig. 3(a)] was comprised of a quadrupole doublet arising from $Fe^{3+}(T_d)$, the spectra of heat-treated samples [Fig. 3(b)–3(m)] showed several peaks as a consequence of magnetic hyperfine structure (hfs). The absorption area arising from magnetic hyperfine structure, A_{hfs}, increased linearly with the heat treatment time; *e.g.*, from 44% [Fig. 3(b)] to 85% [Fig. 3(m)], as illustrated in Fig. 4. Fig. 3 shows that A_{hfs} increased at the expense of the quadrupole doublet which was originally located at 0.21_5 mm s^{-1}. Two types of doublet were observed in Fig. 3(b)–(m), the outer being assigned to $Fe^{3+}(T_d)$ occupying Al^{3+} sites of mayenite. Values of δ and Δ of the outer doublet were estimated to be 0.19 ± 0.01 and 1.59 ± 0.02 mm s^{-1}, respectively; δ for the outer doublet was equal to that of original glass, while Δ of the outer doublet was larger. A similar change in the Mössbauer spectra was observed when mayenite particles precipitated in $60CaO{\cdot}35Al_2O_3{\cdot}5Fe_2O_3$ glass after heat treatment.[13] The inner quadrupole doublet in Fig. 3(b)–(m) is assigned to paramagnetic $Fe^{3+}(T_d)$ remaining in the glassy phase. The values of δ and Δ of the inner doublet were estimated to be 0.13 ± 0.01 and 0.89 ± 0.02 mm s^{-1}, respectively. Linewidths (Γ) were estimated to be 0.46 ± 0.02 mm s^{-1} for both the outer and inner doublets, and were smaller than that of the original glass (0.60 mm s^{-1}). Smaller Γ reflects uniform Fe—O bond lengths and O—Fe—O bond angles. Mössbauer spectra of heat-treated aluminoferrate samples indicate that paramagnetic $Fe^{3+}(T_d)$ substitutes $Al^{3+}(T_d)$ in the glassy phase and mayenite particles.

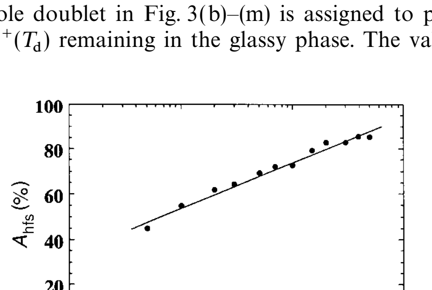

Fig. 4 Change of the relative absorption area of the magnetic hyperfine structure (A_{hfs}) in the Mössbauer spectra of $60CaO{\cdot}27Al_2O_3{\cdot}13Fe_2O_3$ after heat treatment at 750 °C (Fig. 3)

It is considered that the size of the magnetic particles precipitated in the glassy phase is >10 nm, since magnetic hyperfine structure (hfs) is not generally observed when the mean diameter of the magnetic particles is <10 nm.[21] A linear increase of A_{hfs} (Fig. 4) reflects the growth of magnetic particles of $Ca_2Fe_2O_5$. The hfs was analyzed as two sextets: one arising from $Fe^{3+}(O_h)$ with a larger internal magnetic field (H_{int}) of 45 T and the other from $Fe^{3+}(T_d)$ with H_{int} of 39 T. Values of δ for the sextets arising from $Fe^{3+}(O_h)$ and $Fe^{3+}(T_d)$ were estimated to be 0.38 ± 0.02 and 0.21 ± 0.02 mm s^{-1}, respectively, reflecting a high degree of covalency of the Fe^{3+}—O bonds. Values of Δ for $Fe^{3+}(O_h)$ and $Fe^{3+}(T_d)$ were estimated to be 0.61 ± 0.02 and -0.36 ± 0.02 mm s^{-1}, respectively. Fig. 3 reveals that Fe^{3+} ions occupy both O_h and T_d sites in the nanocrystals of $Ca_2Fe_2O_5$, although they occupied tetrahedral NWF sites in the original glass. Larger Γ values of 0.72 ± 0.02 and 1.07 ± 0.02 mm s^{-1} were obtained for $Fe^{3+}(O_h)$ and $Fe^{3+}(T_d)$, respectively, because of the magnetic relaxation effect and also because $Al^{3+}(T_d)$ substituted $Fe^{3+}(T_d)$ in the $Ca_2Fe_2O_5$ particles. Substitution of Al^{3+} for Fe^{3+} in $Ca_2Fe_2O_5$ particles is discussed below.

It is known that in single crystals of dicalcium ferrite, $Ca_2Fe_2O_5$, there are equal numbers of $Fe^{3+}(O_h)$ and $Fe^{3+}(T_d)$, and all the magnetic spins are arranged in an antiparallel direction to each other.[15,19] Smith[20] revealed that $Ca_2Fe_{2-x}Al_xO_5$ can be a solid solution when x is in the range 0–1.36. $Ca_2Fe_{2-x}Al_xO_5$ has an orthorhombic structure with space group *Pcmm* in the range $0\leqslant x\leqslant0.66$, whereas it has space group *Icmm* in the range $0.66\leqslant x\leqslant1.36$. Pobell and Wittmann[14] revealed that $Al^{3+}(T_d)$ preferentially substituted $Fe^{3+}(T_d)$ in the $Ca_2Fe_{2-x}Al_xO_5$ solid solution because the ionic radius of Al^{3+} is slightly smaller than that of Fe^{3+}. Fig. 3 shows that A_{hfs} of $Fe^{3+}(T_d)$ was smaller than that of $Fe^{3+}(O_h)$; this is because $Al^{3+}(T_d)$ preferentially occupies $Fe^{3+}(T_d)$ sites in nanocrystals of $Ca_2Fe_2O_5$, as observed in the solid solution of $Ca_2Fe_{2-x}Al_xO_5$.[14] A $Ca_2Fe_{2-x}Al_xO_5$ solid solution with $x=1.0$ is termed brownmillerite.

Grant and co-workers[16,17] measured a Néel temperature (T_N) of 457±2 °C for $Ca_2Fe_2O_5$, which decreased monotonously when Fe^{3+} was replaced by Ga^{3+} or Sc^{3+}. From the temperature dependency of H_{int} in the Mössbauer spectra, Eibschütz *et al.*[19] determined T_N of $Ca_2Fe_2O_5$ to be 452 °C. Values of H_{int} of 52 and 44 (±0.5) T obtained at room temperature decreased with increasing temperature and reached 0 T at T_N. Smaller H_{int} values of 45 and 39 T obtained in Fig. 3 are ascribed to the smaller size of the crystalline particles (nanocrystals) precipitated in the glassy phase. Grant[18] determined the electric field gradient (e^2qQ) at the nuclear site of Fe^{3+} in single crystals of $Ca_2Fe_{2-x}Al_xO_5$ ($x=0$ or 1.0). He elucidated that the sign of electric field tensor along the *z*-axis, *i.e.*, V_{zz}, was positive at $Fe^{3+}(O_h)$ sites, but negative at $Fe^{3+}(T_d)$ sites. This is consistent with the sign of Δ obtained for the sextets in Fig. 3.

$Ca_2Fe_2O_5$ is known to be antiferromagnetic,[15–19] as described above. The molar magnetic susceptibilities, χ_m, were measured for both the original glass and heat-treated samples. Fig. 5(a) illustrates $\chi_m T$ values of $60CaO·27Al_2O_3·13Fe_2O_3$ glasses at several temperatures (T) between 78 and 298 K. Fig. 5(a) shows an almost linear curve reflecting paramagnetic Fe^{3+}. This is consistent with the Mössbauer spectra of the $60CaO·27Al_2O_3·13Fe_2O_3$ glass [Fig. 3(a)], which showed only one 'paramagnetic' quadrupole doublet. All the $\chi_m T$ values of the samples heat treated for 2000 [Fig. 5(b)] and 5000 min [Fig. 5(c)] at 750 °C were smaller than those of the original glass. The $\chi_m T$ values of heat-treated samples showed a downward bending at low temperature. These results are consistent with the precipitation of antiferromagnetic $Ca_2Fe_2O_5$ particles.

Values of $\chi_m T$ for heat-treated $25K_2O·65V_2O_5·10Fe_2O_3$ samples are illustrated in Fig. 5(d)–5(f), for comparison with our samples. 'Paramagnetic' vanadate glass [Fig. 5(d)] showed an overall decrease of $\chi_m T$ values after heat treatment at 340 °C for 2100 [Fig. 5(e)] and 5000 min [Fig. 5(f)] due to antiferromagnetic interactions of $Fe^{3+}(T_d)$ ions.[22] For $25K_2O·65V_2O_5·10Fe_2O_3$ glass, a Curie–Weiss constant (θ) of −13 K was obtained from the intercept of the straight line in a plot of $1/\chi_m$ *vs.* T. The value of θ decreased from −13 to −93 and −108 K after heat treatment at 340 °C for 2100 and 5000 min, respectively, owing to the precipitation of KV_3O_8 particles. For the $60CaO·27Al_2O_3·13Fe_2O_3$ glass sample [Fig. 5(a)], a plot of $1/\chi_m$ *vs.* T yielded a θ value of −50 K. The Curie–Weiss law could not be applied to heat-treated samples [Fig. 5(b), 5(c)] because the plot yielded a curve instead of a straight line. By using eqn. (3), the effective magnetic moment (μ_{eff}) of $60CaO·27Al_2O_3·13Fe_2O_3$ glass was calculated to be 2.0 μ_B at 298 K.

The value of μ_{eff} decreased linearly with decreasing temperature and reached 1.8 μ_B at 80 K. The μ_{eff} values of the $60CaO·27Al_2O_3·13Fe_2O_3$ sample heat treated at 750 °C for 2000 and 5000 min were calculated to be 1.5–1.7 and 1.4–1.7 μ_B, respectively, in the same temperature region (80–298 K). It is noted that larger μ_{eff} values of 5.5–5.8 μ_B were obtained for $25K_2O·65V_2O_5·10Fe_2O_3$ glass in the region 80–300 K.[22] The μ_{eff} values of vanadate samples heat treated at 340 °C for 2100 min were estimated to be 4.0–5.4 μ_B in the region 80–298 K.[22] After additional heat treatment at 340 °C for 3000 min, μ_{eff} decreased to 3.9–5.2 μ_B in the same temperature region. The decrease of μ_{eff} from 5.5–5.8 to 3.9–5.2 μ_B evidently shows an 'antiferromagnetic' interaction of Fe^{3+} spins in a 'paramagnetic' glass sample.

Fig. 6 illustrates a change of the IR transmittance of $60CaO·27Al_2O_3·13Fe_2O_3$ samples after heat treatment at 760 °C for 0–1000 min. The IR transmittance (T) showed a systematic decrease from 26 to 8% along with the precipitation of dicalcium ferrite ($Ca_2Fe_2O_5$) and mayenite ($12CaO·7Al_2O_3$). Since the decrease of T is ascribed to scattering or reflection of the incident light, the decrease of T can be related with the fraction of crystalline particles precipitated in the glassy phase. Fig. 6 indicates that a distinct decrease of T was observed when the glass sample was heat treated for several minutes. This result is consistent with the Mössbauer spectra [Fig. 3(b)–3(m)], in which magnetic hyperfine structure of antiferromagnetic $Ca_2Fe_2O_5$ particles with a mean diameter > 10 nm appeared after heat treatment.

A Johnson–Mehl–Avrami (JMA) plot [eqn. (1)] was applied to a $60CaO·27Al_2O_3·13Fe_2O_3$ sample in order to estimate the activation energy (E_a) and the mechanism of crystallization. An Avrami index (n) of 1.2 was obtained from the slope of the straight line in the JMA plot (Fig. 7), reflecting two- or three-

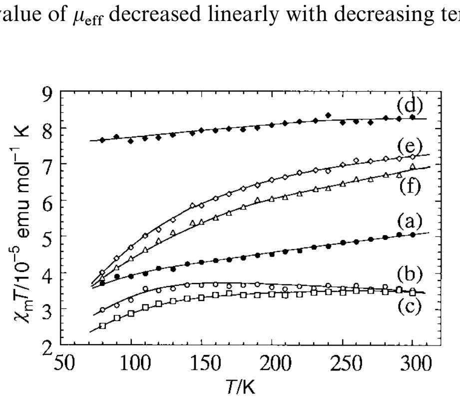

Fig. 5 $\chi_m T$ values of the $60CaO·27Al_2O_3·13Fe_2O_3$ sample plotted *vs.* temperature (T), in which χ_m is the molar magnetic susceptibility. Heat treatment of the sample was conducted at 750 °C for (a) 0, (b) 2000 and (c) 5000 min. $\chi_m T$ values of the $25K_2O·65V_2O_5·10Fe_2O_3$ sample[22] after heat treatment at 340 °C for (d) 0, (e) 2100 and (f) 5000 min are shown for comparison.

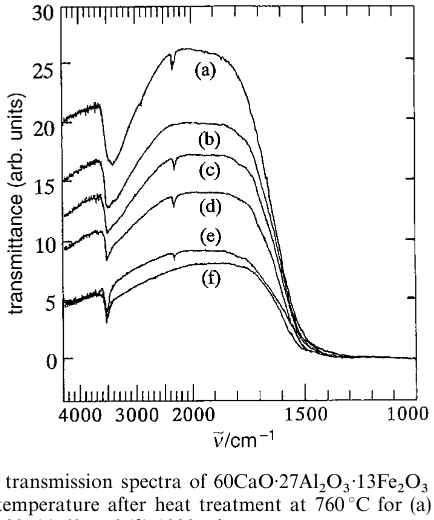

Fig. 6 IR transmission spectra of $60CaO·27Al_2O_3·13Fe_2O_3$ measured at room temperature after heat treatment at 760 °C for (a) 0, (b) 15, (c) 20, (d) 30, (e) 60 and (f) 1000 min

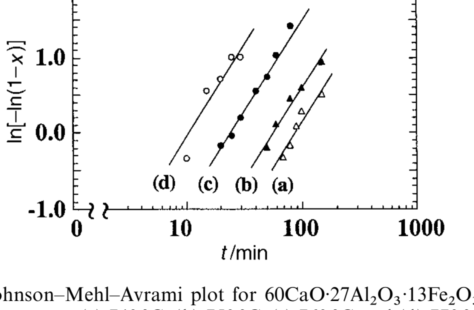

Fig. 7 Johnson–Mehl–Avrami plot for $60CaO·27Al_2O_3·13Fe_2O_3$ after heat treatment at (a) 740 °C, (b) 750 °C, (c) 760 °C and (d) 770 °C. $n=1.2$, $E_a=4.9\pm0.4$ eV.

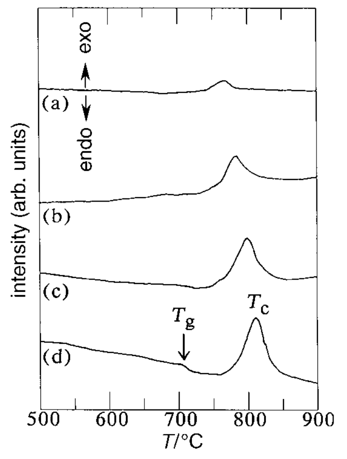

Fig. 8 DTA curves of $60CaO·27Al_2O_3·13Fe_2O_3$ glass recorded at heating rates of (a) 2, (b) 5, (c) 10 and (d) 15 °C min^{-1}

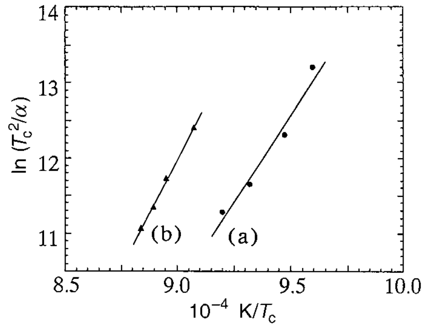

Fig. 9 Kissinger plot for (a) $60CaO·27Al_2O_3·13Fe_2O_3$ (E_a = 4.2 ± 0.3 eV) and (b) $60CaO·35Al_2O_3·5Fe_2O_3$ (E_a = 4.6 ± 0.3 eV) glasses

dimensional crystallization by a diffusion process. The value E_a was estimated to be 4.9 ± 0.4 eV from the Arrhenius plot of rate constants (k) obtained from the intercept of JMA plot. A comparable E_a of 4.3 ± 0.4 eV was previously obtained from the JMA plot of $60CaO·35Al_2O_3·5Fe_2O_3$ glass,[4] together with an Avrami index (n) of 1.5 which reflected three-dimensional crystallization by a diffusion process.

In order to obtain E_a values from Kissinger plots, DTA measurements were carried out for the $60CaO·27Al_2O_3·13Fe_2O_3$ glass. As shown in Fig. 8, T_c showed a systematic increase from 769 to 783, 800 and 814 °C when DTA was conducted at heating rates of 2, 5, 10 and 15 °C min^{-1}, respectively. The slope of the straight line in the Kissinger plot [Fig. 9(a)] yielded E_a of 4.2 ± 0.3 eV for the $60CaO·27Al_2O_3·13Fe_2O_3$ glass. A Kissinger plot for a $60CaO·35Al_2O_3·5Fe_2O_3$ glass is shown in Fig. 9(b) for comparison, which yielded E_a of 4.6 ± 0.3 eV. These values are equal to the values of E_a obtained from JMA plots of $60CaO·27Al_2O_3·13Fe_2O_3$ glass (*i.e.* 4.9 ± 0.4 eV) and $60CaO·35Al_2O_3·5Fe_2O_3$ glass (*i.e.* 4.3 ± 0.4 eV[4]).

All the E_a values obtained for $60CaO·27Al_2O_3·13Fe_2O_3$ and $60CaO·35Al_2O_3·5Fe_2O_3$, *i.e.* 4.2 ± 0.3–4.9 ± 0.4 eV, are comparable to Al—O single bond energy of 4.4 eV.[23] This result indicates that crystallization of calcium aluminoferrate glass is triggered by cleavage of Al—O bonds accompanying a precipitation of the particles of $12CaO·7Al_2O_3$ at an early stage. A similar type of crystallization mechanism was observed in $60CaO·39Ga_2O_3·Fe_2O_3$[1] and $95TeO_2·5Fe_2O_3$ glasses,[2] for which JMA plots yielded E_a of 3.3 ± 0.4 and 2.9 ± 0.4 eV, respectively. Since these values were comparable to the Ga—O (2.9 eV[23]) and Te—O bond energies (3.0 eV[23]), respectively, it was concluded that cleavage of Ga—O and Te—O bonds triggered the crystallization. Kissinger plots of $38Na_2O·62WO_3$ and $38Na_2O·61WO_3·Fe_2O_3$ glasses yielded E_a of 4.7 ± 0.3 and 2.6 ± 0.3 eV, respectively.[11] The former value was equal to the W—O single bond energy of 4.5 eV,[23] while the latter corresponded to the Fe—O single bond energy. This result indicates that cleavage of W—O and Fe—O bonds triggered the crystallization of iron-free and iron-containing tungstate glasses, respectively. In addition, comparable E_a values of 2.0 ± 0.3–2.9 ± 0.3 eV were obtained from the Kissinger plots of $xK_2O·(90-x)V_2O_5·10Fe_2O_3$ glasses (x = 20–30),[22] which were much smaller than the V—O single bond energy of 3.9 eV.[23] These results indicate that crystallization of tungstate and vanadate glasses containing iron was triggered by cleavage of Fe—O bonds. Since the E_a of 4.2 ± 0.3–4.9 ± 0.4 eV obtained for $60CaO·27Al_2O_3·13Fe_2O_3$ and $60CaO·35Al_2O_3·5Fe_2O_3$ glasses are much larger than the Fe—O bond energy, it is considered that cleavage of Fe—O bonds plays no significant role in the crystallization of aluminoferrate glass; Fe^{3+} behaves in the same manner as Al^{3+} throughout the crystallization process and occupies substitutional sites of Al^{3+} in the original glass and also in the particles of $12CaO·7Al_2O_3$. Similarly, Al^{3+} substitutes Fe^{3+} in the particles of $Ca_2Fe_2O_5$, as confirmed from the Mössbauer spectra (Fig. 3).

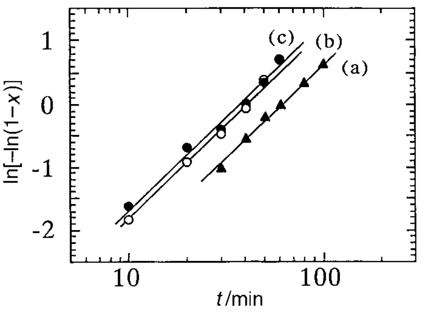

Fig. 10 Johnson–Mehl–Avrami plot for $60CaO·40Al_2O_3$ heat treated at (a) 830, (b) 850 and (c) 860 °C. n = 1.5, E_a = 5.6 ± 0.4 eV.

A JMA plot in the IR-transmission method was applied to iron-free $60CaO·40Al_2O_3$ glass in order to investigate the crystallization mechanism. The slope of the straight line (n) in the JMA plot (Fig. 10) was estimated to be 1.5, which reflected a three-dimensional crystallization proceeding from the surface to the bulk by a diffusion process. An Arrhenius plot of the k values obtained from JMA plots of $60CaO·40Al_2O_3$ glass yielded an E_a value of 5.6 ± 0.3 eV. Also, a Kissinger plot in the DTA method was applied to $60CaO·40Al_2O_3$ glass in order to estimate E_a. The T_c of $60CaO·40Al_2O_3$ glass shifted from 926 to 940, 948 and 955 °C when the heating rate (α) was increased from 5 to 10, 15 and 20 °C min^{-1}, respectively. The T_c values of 769–814 °C obtained for the $60CaO·27Al_2O_3·13Fe_2O_3$ glass are much lower than those of $60CaO·40Al_2O_3$ glass (926–955 °C), indicating that substi-

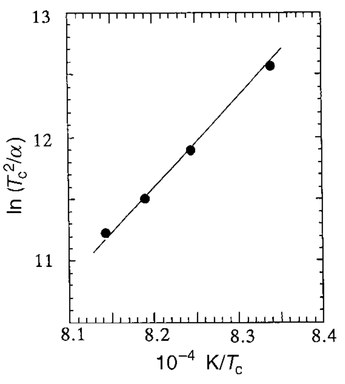

Fig. 11 Kissinger plot for $60CaO·40Al_2O_3$ glass (E_a = 6.0 ± 0.3 eV)

tution of Fe^{3+} for Al^{3+} brings about a systematic lowering of T_c (and also T_g) by more than 100 °C. A Kissinger plot obtained for the $60CaO{\cdot}40Al_2O_3$ glass is illustrated in Fig. 11. An E_a of 6.0 ± 0.3 eV was obtained from the slope of the straight line, which was equal to the E_a obtained from the JMA plot of Fig. 10. Since the E_a values of 5.6 ± 0.4 and 6.0 ± 0.3 eV are equal to a sum of the Al—O (4.4 eV[23]) and Ca—O bond energies (1.4 eV[23]), it is considered that simultaneous cleavage of Al—O and Ca—O bonds takes place at an early stage of crystallization, accompanying the precipitation of $12CaO{\cdot}7Al_2O_3$ particles.

Conclusions

(1) Heat treatment of $60CaO{\cdot}27Al_2O_3{\cdot}13Fe_2O_3$ glass resulted in a precipitation of nanocrystals of mayenite ($12CaO{\cdot}7Al_2O_3$) and antiferromagnetic dicalcium ferrite ($Ca_2Fe_2O_5$), which caused a decrease of the effective magnetic moment (μ_{eff}) from 1.8–2.0 to 1.4–1.7 μ_B.

(2) $Fe^{3+}(T_d)$ substitutes $Al^{3+}(T_d)$ in $60CaO{\cdot}27Al_2O_3{\cdot}13Fe_2O_3$ glass, and Fe^{3+} behaves in the same manner as Al^{3+} throughout the crystallization. The $Fe^{3+}(T_d)$ substitutes $Al^{3+}(T_d)$ in the particles of $12CaO{\cdot}7Al_2O_3$, while $Al^{3+}(T_d)$ substitutes $Fe^{3+}(T_d)$ in $Ca_2Fe_2O_5$ particles.

(3) Internal magnetic fields (H_{int}) for $Fe^{3+}(O_h)$ and $Fe^{3+}(T_d)$ in $Ca_2Fe_2O_5$ particles were estimated to be 45 and 39 T, respectively. The H_{int} values were smaller than those of a $Ca_2Fe_2O_5$ single crystal because of a smaller particle size (*ca.* 10 nm).

(4) Precipitation of $12CaO{\cdot}7Al_2O_3$ and $Ca_2Fe_2O_5$ particles caused a decrease in the IR transmittance due to a scattering or reflection of the incident light. The IR-transmission method revealed that crystallization proceeded in a two- or three-dimensional manner by a diffusion process.

(5) Activation energies (E_a) of 4.2 ± 0.3 and 4.9 ± 0.4 eV estimated for the crystallization of $60CaO{\cdot}27Al_2O_3{\cdot}13Fe_2O_3$ glass were nearly equal to the Al—O bond energy of 4.4 eV, within the experimental error. This result indicates that cleavage of Al—O bonds triggered the formation of $12CaO{\cdot}7Al_2O_3$ particles containing iron.

(6) After prolonged heat treatment, Mössbauer spectra showed an increase in the absorption area of sextets due to $Ca_2Fe_2O_5$ particles at the expense of doublets. This reflects a migration of $Fe^{3+}(T_d)$ from $12CaO{\cdot}7Al_2O_3$ and the glassy phase to $Ca_2Fe_2O_5$ particles.

(7) Values of E_a of 5.6 ± 0.4 and 6.0 ± 0.3 eV were obtained for the crystallization of $60CaO{\cdot}40Al_2O_3$ glass. Since they are equal to a sum of Al—O (4.4 eV) and Ca—O bond energies (1.4 eV), it is concluded that simultaneous cleavage of Al—O and Ca—O bonds triggered the formation of $12CaO{\cdot}7Al_2O_3$.

One of the authors (T.N.) is indebted to Grant-in-Aid for Scientific Research (C) from the Ministry of Education, Science, Sports and Culture.

References

1 T. Nishida, T. Ichii and Y. Takashima, *J. Mater. Chem.*, 1992, **2**, 733.
2 T. Nishida, S. Inoue and Y. Takashima, *Bull. Chem. Soc. Jpn.*, 1992, **65**, 1927.
3 T. Nishida, S. Kubuki and Y. Takashima, *J. Non-Cryst. Solids*, 1994, **177**, 193.
4 T. Nishida and Y. Takashima, *Nucl. Instrum. Methods Phys. Res. B*, 1993, **76**, 397.
5 H. E. Kissinger, *Anal. Chem.*, 1957, **29**, 1702.
6 T. Nishida, *J. Non-Cryst. Solids*, 1994, **177**, 257.
7 T. Nishida, *J. Radioanal. Nucl. Chem.*, 1994, **182**, 451.
8 T. Nishida, *Hyperfine Interact.*, 1995, **95**, 23.
9 T. Nishida, in *Mössbauer Spectroscopy of Sophisticated Oxides*, Akadémiai Kiadó, Budapest, 1997, ch. 2, pp. 27–87.
10 T. Nishida, *Z. Naturforsch., Teil A*, 1996, **51**, 620.
11 T. Nishida, M. Suzuki, S. Kubuki, M. Katada and Y. Maeda, *J. Non-Cryst. Solids*, 1996, **194**, 23.
12 G. Adams and J. H. Gibbs, *J. Chem. Phys.*, 1965, **43**, 139.
13 T. Nishida, H. Ide, T. Shinmyozu, Y. Takashima and Y. Matsumoto, *Jpn. J. Appl. Phys.*, 1990, **29**, 1293.
14 F. Pobell and F. Wittmann, *Phys. Lett.*, 1965, **19**, 175.
15 S. Geller, R. W. Grant, U. Gonser, H. Wiedersich and G. P. Espinosa, *Phys. Lett.*, 1966, **20**, 115.
16 R. W. Grant, H. Wiedersich, S. Geller, U. Gonser and G. P. Espinosa, *J. Appl. Phys.*, 1967, **38**, 1455.
17 S. Geller, R. W. Grant, U. Gonser, H. Wiedersich and G. P. Espinosa, *Phys. Lett. A*, 1967, **25**, 722.
18 R. W. Grant, *J. Chem. Phys.*, 1969, **51**, 1156.
19 M. Eibschütz, U. Ganiel and S. Shtrikman, *J. Mater. Sci.*, 1969, **4**, 574.
20 D. K. Smith, *Acta Crystallogr.*, 1962, **15**, 1146.
21 N. N. Greenwood and T. C. Gibb, in *Mössbauer Spectroscopy*, Chapman and Hall, London, 1971, ch. 10.
22 T. Nishida, J. Kubota, Y. Maeda, F. Ichikawa and T. Aomine, *J. Mater. Chem.*, 1996, **6**, 1889.
23 D. Chakravorty, in *Modern Aspects of Solid State Chemistry*, Plenum Press, New York, 1980, pp. 391–423.

Paper 7/02854G; *Received* 28*th April* 1997